THE JOURNAL OF PHYSICAL CHEMISTRY C
A JOURNAL OF THE AMERICAN CHEMICAL SOCIETY

Open Access
This article is licensed under CC-BY 4.0

pubs.acs.org/JPCC
Article

First-Principles Study of $Sr_{2-x}La_xFeO_4$ and Comparison with $Sr_2FeO_{4-\delta}$: The Nature of the Positively Charged Defect Determines the Character of the Electronic Structure

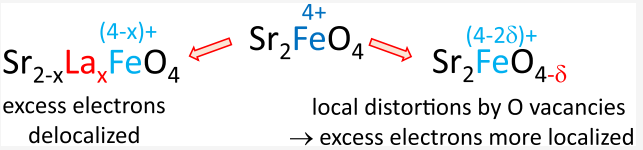
Yuri A. Mastrikov,* Denis Gryaznov,* Andrew Chesnokov, Guntars Zvejnieks, Maksim Sokolov, Maija M. Kuklja, Rotraut Merkle,* and Eugene Kotomin

Cite This: J. Phys. Chem. C 2026, 130, 11001−11008

Read Online

ACCESS | Metrics & More | Article Recommendations | Supporting Information

ABSTRACT: Lanthanum doping of the first-order Ruddlesden−Popper (RP) phases $Sr_{2-x}La_xFeO_4$ ($0 \le x \le 1$) is investigated by density functional theory (DFT) calculations. Excess volume and excess energy of this solid solution series are calculated. The evolution of the electronic structure with increasing La content is discussed based on the calculated Fe magnetic moment. It is found that for the same average Fe oxidation state, the electronic structure in $Sr_{2-x}La_xFeO_4$ displays a more delocalized character than in corresponding $Sr_2FeO_{4-\delta}$ composition. This is attributed to the fact that oxygen vacancies $V_O^{\bullet\bullet}$ which are formed under Fe−O bond breaking (and which carry a doubly positive charge) represent a stronger local distortion than singly charged substitutional $La_{Sr}^{\bullet}$ dopants.



1. INTRODUCTION

The group of strontium ferrate perovskites and perovskite-related oxides is a fascinating material class. On one hand, it is interesting from a fundamental point of view, because different geometrical and electronic structures have very close energies so that delicate interactions finally decide which one becomes most stable. For the first-order Ruddlesden−Popper (RP) phase Sr_2FeO_4, magnetic structure measurements indicated a symmetry reduction from the tetragonal phase,[1] and computational investigations also identified a symmetry reduction to orthorhombic and interpreted it as a Jahn−Teller (JT) distortion.[2,3] In the second-order RP phase $Sr_3Fe_2O_7$, the energy difference between a charge-ordered state (with Fe^{3+} and Fe^{5+}) and a JT-distorted state is on the order of only 34 meV/formula unit, as found by the hybrid r²SCANh calculations.[4]

Overall, the electronic structure of $Sr_{n+1}Fe_nO_{3n+1\pm\delta}$ RP phases has a more localized character than that of the simple perovskite $SrFeO_{3-\delta}$ (indicated, e.g., by the fact that the vacancy formation energy is almost constant in $Sr_2FeO_{4-\delta}$,[2] while it strongly increases with increasing δ in $SrFeO_{3-\delta}$[5]). This is to some degree simply related to the transition from a 3- to a 2-dimensional system. However, the comparison of $Sr_2FeO_{4-\delta}$ and $Sr_{2-x}La_xFeO_4$ in the present investigation demonstrates that also the nature of the introduced positively charged defect (oxygen vacancies, or La^{3+} substituting for Sr^{2+}) plays an important role. These defects not only decrease the average Fe oxidation state but also affect the character of the electronic structure. Introducing oxygen vacancies results in a rather localized character where—from a combination of Fe−O bond lengths and Fe magnetic moments—iron atoms with integer Fe^{3+} and Fe^{4+} oxidation states could be recognized.[1] In the present study, we investigate the effects of La doping in $Sr_{2-x}La_xFeO_4$, which will be shown to result in a more delocalized character.

The character of the Fe−O bonding is not only of fundamental interest but also directly affects the material's properties regarding proton incorporation. Redox-active perovskites and perovskite-related materials serve as hole-oxygen vacancy mixed conducting or even proton-hole-vacancy triple conducting air electrode materials in solid oxide cells and protonic ceramic cells.[6−8] Compared to ABO_3 simple perovskites and $AA'B_2O_6$ or $A_2BB'O_6$ double perovskites, RP phases comprise a higher fraction of *A*-site cations, which is expected to increase the overall basicity of the material. Further, the fraction of alkali earth (2+) and rare earth (3+) cations on the *A*-site affects the properties. Sr_2FeO_4 is an aristotype for the first-order RP phases utilized as mixed conducting electrode materials in ceramic electrochemical cells.[9−11] While Sr_2FeO_4 itself needs to be prepared under high oxygen pressure,[12] higher-order RP phases $Sr_{n+1}Fe_nO_{3n+1\pm\delta}$ or rare-earth doped compositions can be prepared under ambient conditions, e.g., $Sr_3Fe_2O_7$[13,14] or $SrEu_2Fe_2O_7$.[15] Besides Fe-based RP phases, also Co- and in particular Ni-based materials have been

Received: December 30, 2025
Revised: June 25, 2026
Accepted: June 26, 2026
Published: July 28, 2026



ACS Publications
© 2026 The Authors. Published by American Chemical Society

https://doi.org/10.1021/acs.jpcc.5c08764
J. Phys. Chem. C 2026, 130, 11001−11008

Downloaded from http://pubs.acs.org/jpccck/article-pdf/130/31/11001/6305266/acs.jpcc.5c08764.pdf by guest on 09 August 2026

investigated as air electrode materials for protonic ceramic cells, e.g., $(La,Sr_3)Co_{1.5}Fe_{1.5}O_{10}$,[16] $(Pr,Sr)_2NiO_4$,[17] $(La,Sr)_2NiO_4$,[18] $(Ba,Sr,La)_2NiO_4$,[19] or oxygen storage materials $Sr_3Fe_{2-x}Ni_xO_{7-\delta}$.[20] Here, we concentrate on Fe-based $Sr_{2-x}La_xFeO_4$, RP phases where we can compare with the preceding computational work with the same methodological approach for $Sr_2FeO_{4-\delta}$ and $SrFeO_{3-\delta}$.[2,5,21] While both oxygen vacancies and La dopants are positive defects (charge-compensated by a decrease of the average iron oxidation state), the present results indicate that they modify the electronic structure of the material in different ways. This comparison enhances the general understanding of the defect chemistry of mixed conducting oxides, particularly in delicate situations as encountered in the Ruddlesden–Popper oxides where the energetic difference between more or less localized electronic defects is small.

2. METHOD AND MODEL

Doping $Sr_2FeO_{4-\delta}$ by La has been performed by substitution $La^{\bullet}_{Sr}$. La concentration x has been varied from 0.125 up to 1.00. Varying x continuously, we minimize the possibility of technical errors in calculations and ensure the integrity of the results within the range of interest. The supercell of eight Sr_2FeO_4 formula units (56 atoms) is suitable for modeling a relatively low La concentration (x = 0.125). Only one inequivalent configuration of La_{Sr} is possible in a model supercell. For higher values of x, all possible spatial distributions of La_{Sr} have been investigated (Table S1) by means of the Supercell code.[22] Screening of this large number of configurations proved necessary because the lowest energy configuration for a given La content in the supercell does not necessarily occur for the intuitively guessed arrangements with maximum La distances (cf. discussion of Figures 2 and S1). Note that representability of a particular configuration depends on its energy, multiplicity, and structural stability. Calculations have been performed by the computer code VASP.[23] Effects of core electrons were emulated by PAW[24] potentials (Table S2). Computational details are presented in Table 1. The Hubbard correction value U_{eff} = 4 eV has been chosen based on an extensive analysis of structural and electronic parameters of $SrFeO_3$ and Sr_2FeO_4.[2] In addition to that, the value has been considered optimal for similar $(Ba,Sr)FeO_{3-\delta}$ and $(Pr,Sr)_2FeO_{4-\delta}$ perovskites.[21,25,26]

Table 1. Main Computational Parameters

computer code	VASP 6.1.2
cutoff energy	520 eV
space group (SG), Settings	64, *Bbem*
transformation matrix from the crystallographic unit cell to the supercell	$\begin{pmatrix} 1 & 1 & 0 \\ -1 & 1 & 0 \\ 0 & 0 & 1 \end{pmatrix}$
K-points	Monkhorst–Pack[27] 4 × 4 × 2
exchange–correlation functional	Perdew–Burke–Ernzerhof[28]
U_{eff}	4.0 eV
residual external pressure	<1 kbar
forces on atoms	<0.02 eV/Å

Electron charge and magnetic moments were analyzed by the Bader method.[29] Structure visualization was performed using the code VESTA.[30]

Considering one extra electron released to the system by each substitution of Sr^{2+} by La^{3+} ($La^{\bullet}_{Sr}$), and two extra electrons released by an oxygen vacancy, the formal Fe^{3+}/Fe ratio can be defined as follows:

$$Sr_{2-x}La_xFe^{4+}_{1-(2\delta+x)}Fe^{3+}_{2\delta+x}O_{4-\delta} \quad (1)$$

The high covalency of the Fe–O bonds in the system prevents a clear distinction between these two oxidation states of Fe. A direct charge calculation by the Bader method proved to be unreliable for assigning Fe oxidation states. Therefore, for oxidation state identification, we used magnetic moment combined with the lengths of Fe–O bonds, as proposed in ref 2.

3. RESULTS

3.1. Excess Energy, Volume, and Spatial Distribution of $La^{\bullet}_{Sr}$

The energetic stability of a complex material like $Sr_{2-x}La_xFeO_{4-\delta}$ depends on defect (*A*-cation substitution, oxygen vacancy/interstitial) concentration as well as on their spatial distribution. Oxygen defects have been studied in detail in ref 2 In the present work, we focus on $La^{\bullet}_{Sr}$ substitution, preserving the oxygen stoichiometry at δ = 0, except for x = 0.125 (discussed below). The energetic stability of $Sr_{2-x}La_xFeO_4$ was calculated as excess energy relative to the linear interpolation between the La-free composition (x = 0) and the lowest energy state for $x_{ref.}$ = 1.00 (Table S3 and Figure S1d).

$$E_{excess} = E_x - (E_{x=0} + (E_{min\ x=1} - E_{x=0})x) \quad (2)$$

The nonzero excess energies in Figure 1a indicate moderate deviations from an ideal solution. The negative excess energy values indicate an overall driving force for mixing between Sr_2FeO_4 and $SrLaFeO_4$ (the distribution of La and Sr within the cell may still have a preference for the La segregation, see later). Comparison with other perovskite-type materials (Table 2) indicates that a smaller size mismatch and more flexibility in the structural and chemical bonding properties (e.g., presence of more loosely bound rocksalt layers in RP phases) favor the formation of stable solid solutions. The rocksalt AO layer in the RP phase offers even more flexibility to accommodate differently sized *A*-cations (for RP phases of higher orders even with crystallographically different *A*-sites).

Interestingly, the excess energy curve of $Sr_{2-x}La_xFeO_4$ has an asymmetric shape. Compositions with intermediate La content x = 0.5 and x = 0.75 have the most negative excess energies, i.e., the minimum is shifted toward higher La contents. Also, the volume shows moderate deviations from the ideal behavior Figure 1b, but in contrast to the excess energy, the excess volume shows an approximately symmetrical shape. The absolute molar volume increases with increasing La substitution despite La^{3+} (1.36 Å) having a smaller Shannon radius than Sr^{2+} (1.44 Å, both in 12-fold coordination), in line with experimental data.[35] This volume expansion is caused by a decrease in the average Fe oxidation state and an increase in the corresponding Fe ionic radius. The volume expansion between Sr_2FeO_4 and $SrLaFeO_4$ amounts to 2.7%, which is significantly larger than the respective expansion by 1% between Sr_2FeO_4 and $Sr_2FeO_{3.5}$ (also changing from average Fe^{4+} to Fe^{3+}).[2] This results from the fact that in $Sr_{2-x}La_xFeO_4$ the Fe reduction is not accompanied by removal of oxygen ions.

Downloaded from http://pubs.acs.org/jpccck/article-pdf/130/31/11001/6305266/acs.jpcc.5c08764.pdf by guest on 09 August 2026

https://doi.org/10.1021/acs.jpcc.5c08764
J. Phys. Chem. C 2026, 130, 11001–11008

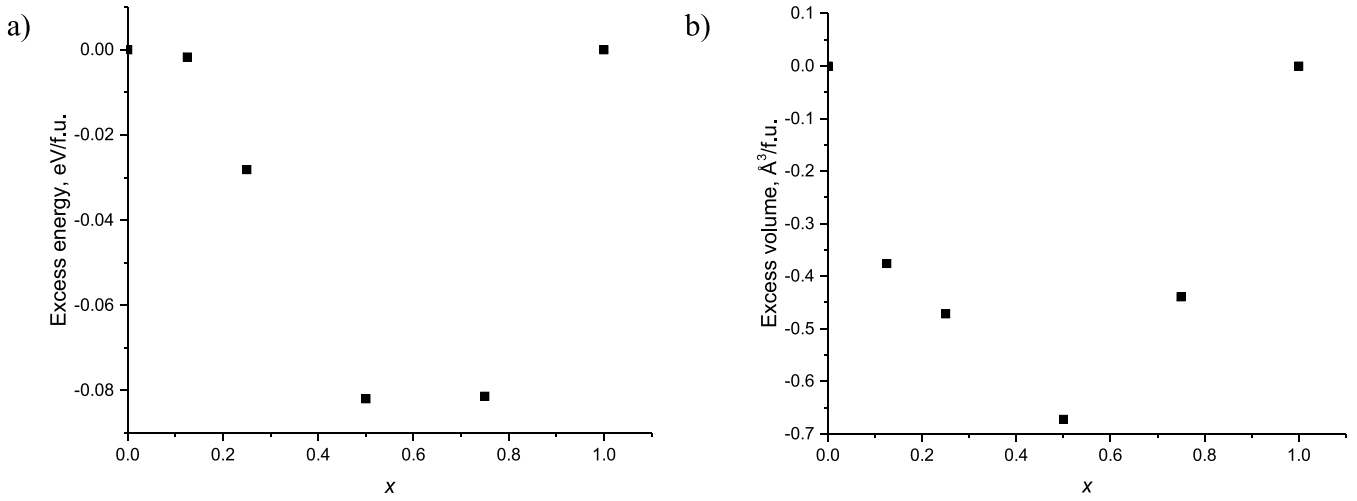


Figure 1. (a) Excess energy (per formula unit) of $Sr_{2-x}La_xFeO_4$. (b) Excess volume (per formula unit) of $Sr_{2-x}La_xFeO_4$. The data correspond to the configurations with the lowest total energy for each La content.

Table 2. Excess Energy for Various Composition Changes in Perovskite-Related Structures: A_2BO_4 and ABO_3

material	structure	mixing cation, size difference, Å	variation	excess energy	source
$Sr_{2-x}La_xFeO_4$	1st order RP	*A* 0.08	atomic radius, oxidation state of A- and B-cations	negative	this study
$La_{1-x}Sr_xCoO_3$	perovskite	*A* 0.08			31
$La_{1-x}Sr_xMnO_3$	perovskite	*A* 0.08			32
$Ba_{1-x}Sr_xTiO_3$	perovskite	*A* 0.17	atomic radius	positive	33
$BaFe_{1-x}Ce_xO_3$	perovskite	*B* 0.28			34

Figure 2 shows that for each La content the lowest energy is found for the configurations with the shortest average La−O distance (configurations shown in Figure S1). These arrangements lead to the most beneficial La^{3+}−O^{2-} electrostatic interactions. A more detailed analysis (Figure S2) indicates the sensitivity for certain detailed structural features (which together finally determine the average La−O distance). Figure S2a demonstrates that for a given *x*, a larger number of $La_{Sr}^{\bullet}$−$La_{Sr}^{\bullet}$ bonds (1NN) across the perovskite layer slightly increases the energy. A larger number of 2NN $La_{Sr}^{\bullet}$−$La_{Sr}^{\bullet}$ bonds lowers the energy (Figure S2b,e,h). Both criteria together correspond to accumulating La within the same rocksalt layer (but distributed over both AO planes of that layer). If several $La_{Sr}^{\bullet}$ are located within the same AO plane, then the configurations with more 3NN pairs are more favorable (Figure S2c). This can be traced back to the fact that this arrangement allows for shorter La−O and longer Sr−O distances reflecting their size as well as charge difference (Figure 3b), in contrast to the case of Figure 3c, where the topology enforces equal—but energetically less favorable—La−O and Sr−O lengths. So, the spatial arrangement does not simply follow the principle of maximizing or minimizing the distance between $La_{Sr}^{\bullet}$ substitutions which carry a relative positive charge compared to Sr.

We also briefly explored the energetics of oxygen-deficient composition $Sr_{1.875}La_{0.125}FeO_{3.875}$ (Table S4). Since $La_{Sr}^{\bullet}$ and $V_O^{\bullet\bullet}$ are both positive defects, it is not surprising to find a moderate positive interaction energy (Figure S4), in the range from 0.2 to 0.8 eV. Since the interaction energy depends only slightly on the actual $La_{Sr}^{\bullet}$−$V_O^{\bullet\bullet}$ distance, the presence of $V_O^{\bullet\bullet}$ is not expected to significantly change the relative stability of different $La_{Sr}^{\bullet}$−$La_{Sr}^{\bullet}$ configurational arrangements for the higher La concentrations. Just like in the case of Sr_2FeO_4,[2] $V_O^{\bullet\bullet}$ forms preferentially in the FeO_2 planes. The lowest $V_O^{\bullet\bullet}$ formation energies in $Sr_{1.875}La_{0.125}FeO_4$ are only slightly higher than in Sr_2FeO_4 (2.60 and 2.35 eV for Sr−$V_O^{\bullet\bullet}$-Fe and Fe−$V_O^{\bullet\bullet}$-Fe, respectively), which is in line with the fact that for $Sr_2FeO_{4-\delta}$ only a minor variation of $V_O^{\bullet\bullet}$ formation energy with an iron oxidation state has been observed.[2]

3.2. Identification of Fe Oxidation States in $Sr_{2-x}La_xFeO_4$

The high degree of covalency of the Fe−O bonds prevents a clear distinguishing between the 4+ and the 3+ oxidation states of Fe. As discussed in more detail in,[2] the Fe−O bonds in the simple perovskite $SrFeO_3$ have a higher charge transfer from the oxide ions to iron and more delocalized character than in Sr_2FeO_4 with the same formal Fe^{4+} oxidation state. Nevertheless, the Fe−O bonds in Sr_2FeO_4 are still far from purely ionic, and thus, the question whether fixed Fe oxidation states can be assigned is not trivial (attempting to use the Bader charges yields inconsistent results). As proposed in,[2] the Fe magnetic moment combined with the lengths of Fe−O bonds can serve as an indirect indicator of the oxidation state (Figure S5). Already for $x = 0.125$ (one extra electron in a supercell), we observed quite a broad distribution of the magnetic moments (Figure 4a); it is not possible to recognize a single Fe cation with a clear 3+ oxidation state where the excess electron is localized (the data points at high magnetic moment ≈3.84 μ_B represent a total of five (2NN + 4 × 1NN) Fe atoms, Table S5). Reference cells which contain only Fe^{3+} have much higher magnetic moments: (i) in $SrLaFeO_4$, the moments amount to 4.25−4.30 μ_B, (ii) in $Sr_2FeO_{4-\delta}$, the moments cover a larger range of 4.05−4.25 μ_B (larger moments for larger δ[2]). In Figure 4a, the corresponding ranges are indicated in dark gray (comparison with $SrLaFeO_4$) and light gray (lower end interpolated according to the La content between $SrLaFeO_4$ and $Sr_2FeO_{4-\delta}$ with low δ). None of the Fe in $Sr_{1.875}La_{0.125}FeO_4$ comes close to the 3+ range. Some Fe are in the lower part of

https://doi.org/10.1021/acs.jpcc.5c08764
J. Phys. Chem. C 2026, 130, 11001−11008

Downloaded from http://pubs.acs.org/jpccck/article-pdf/130/31/11001/6305266/acs.jpcc.5c08764.pdf by guest on 09 August 2026

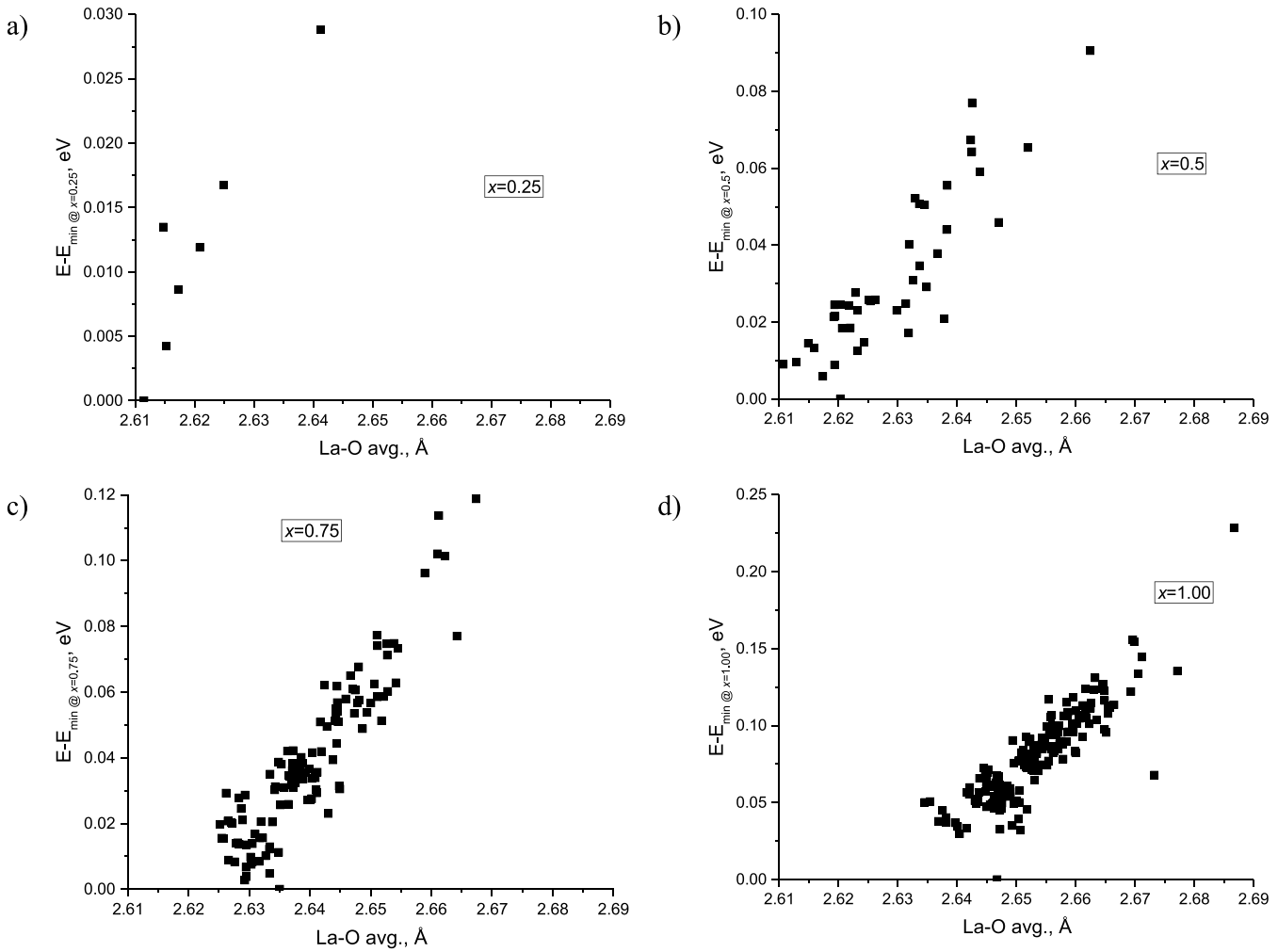


Figure 2. Energy per f.u. relative to the lowest value for each value of x depending on the averaged $La_{Sr}^{\bullet}$−O distance, which is obtained by averaging over the nine La−O bonds around La and all $La_{Sr}^{\bullet}$ cations.

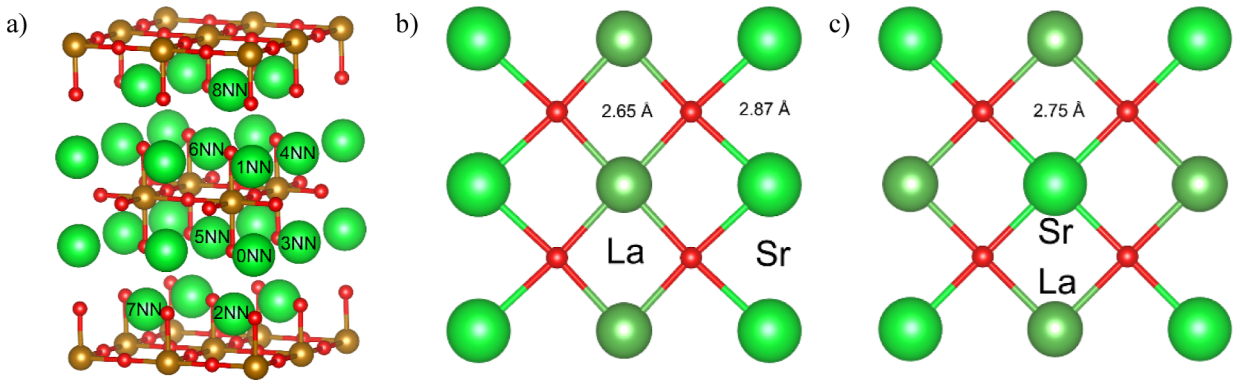


Figure 3. Nearest neighbors (NN) of the A-cation sublattice in the Sr_2FeO_4 RP 1st-order perovskite structure in an 8-formula unit supercell (a). (Note that the periodic boundary conditions are neglected solely for showing the 7NN). La_{Sr} cations in the $Sr_{1.75}La_{0.25}FeO_4$ structure as 3NN (b) and 5NN (c).

the Fe^{4+} reference zone (3.65−3.8 μ_B for Sr_2FeO_4 and $Sr_2FeO_{3.875}$,[2] beige area), while others attain values around 3.85 μ_B. The latter are regarded as a result of delocalization of the excess electron over several iron cations.

For x = 0.25, the situation is closely related (Figure 4b). The configuration with the lowest energy (solid symbols) has only Fe with moments higher than the 4+ reference, i.e., the two excess electrons are homogeneously distributed among all Fe in the cell. However, there are configurations at only slightly higher energy with some Fe^{4+} besides other Fe with decreased oxidation state. For x = 0.5, we see a broad distribution of moments, not touching 3+ and only barely touching the 4+ reference values (Figure 4c). At a high La content of x = 0.75 (average Fe oxidation state 3.25+), the distribution further shifts to higher μ_B values and becomes again narrower (Figure 4d). Finally, for x = 1 (all iron Fe^{3+}), all moments are within

Downloaded from http://pubs.acs.org/jpccck/article-pdf/130/31/11001/6305266/acs.jpcc.5c08764.pdf by guest on 09 August 2026

https://doi.org/10.1021/acs.jpcc.5c08764
J. Phys. Chem. C 2026, 130, 11001−11008

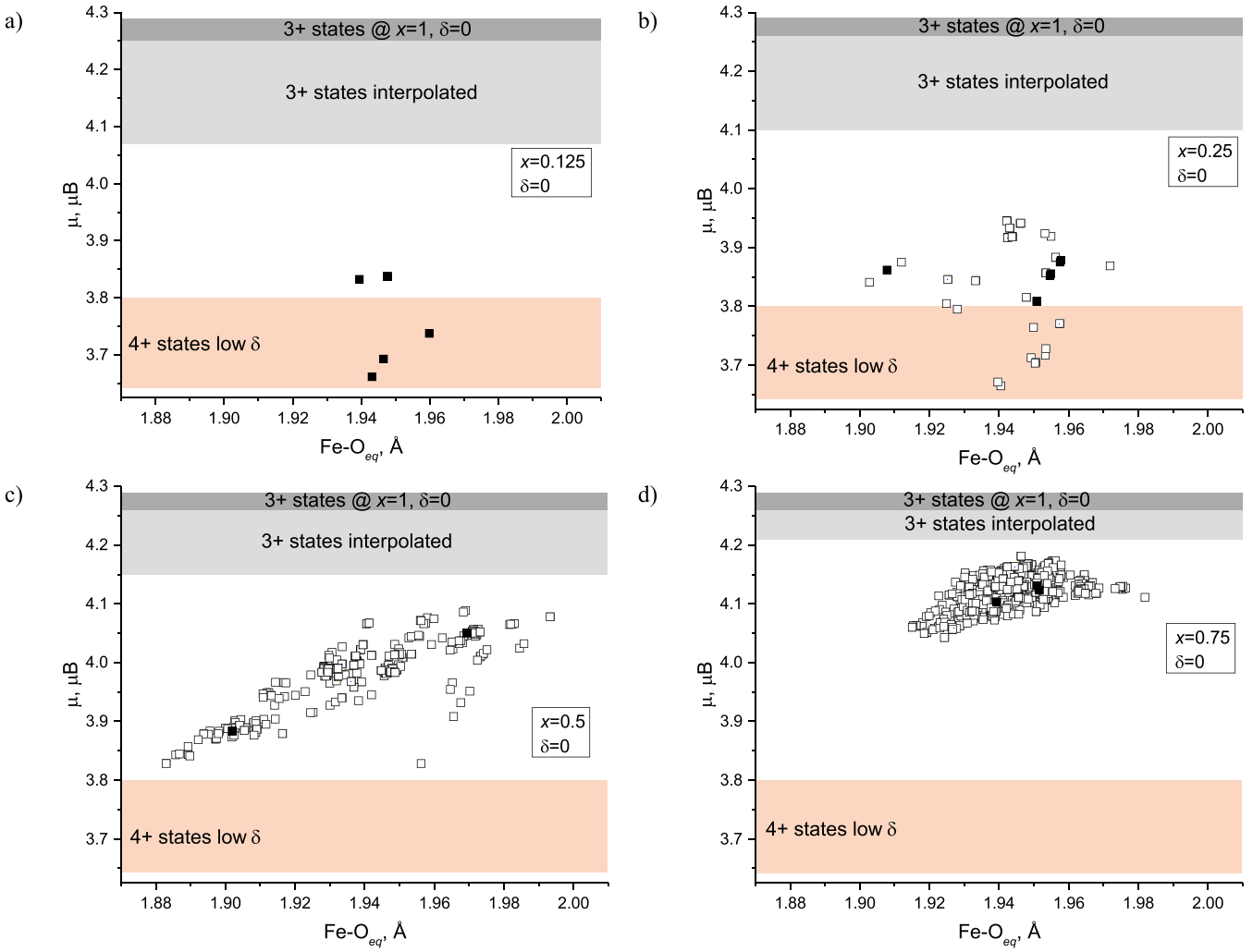


Figure 4. Magnetic moment as a function of averaged Fe−O_{eq} distance (average of the Fe−O_{eq} around each individual Fe in the supercell) for δ = 0 and (a) x = 0.125, (b) x = 0.25, (c) x = 0.5, and (d) x = 0.75. Solid symbols denote the values for the lowest energy configurations. The shaded areas indicate the zones where integer Fe^{3+} and Fe^{4+} oxidation states were assigned for reference configurations. Figure S3 shows the quite similar plots with Fe−O_{ap} and Fe−O (all) on the horizontal axis.

4.25−4.3 μ_B. So, for most of these cases, it is not possible to assign integer 3+ and 4+ oxidation states, and even if some Fe fall into the region of the 4+ state, the excess electron(s) may still be distributed over several other Fe cations.

For x = 0.125 (the composition with the highest tendency to form localized states), we ran extended test calculations attempting to obtain a fully localized polaron (a single Fe^{3+}) by using starting geometries with deliberately distortion Fe−O bond lengths primarily within the DFT + U methodology. However, Table S6 demonstrates that such a solution was not obtained, and further that the energies of partially localized and fully delocalized states are nearly indistinguishable within the accuracy of the method (~4 meV).

To further check the trend of the increasingly delocalized character of the electronic structure with high La content, we also used the HSE06[36] functional to calculate the configurations with the lowest energy (Figure S1) for various La contents (details are given in the Supporting Information). Figure S6 compares the data for the lowest-energy configurations obtained with DFT + U and HSE06. The overall trend of increasing delocalization of the excess electron(s) with increasing La content is observed for both methods. For HSE06, even for the lowest La content, no single Fe^{3+} is found (the maximum magnetic moment remains much below the value expected for Fe^{3+}, and four Fe have an increased magnetic moment, i.e., the excess electron is shared between the 4 × 1NN Fe). A comparison of the electronic density of states (DOS) calculated using DFT + U and the HSE approach is given in Figures S7−S9. Also, here the main trends with varying La content agree well. This is encouraging to see, because HSE calculations are more computationally demanding and more delicate to properly converge.

3.3. Comparison with Sr_2FeO_4

A direct comparison with the earlier studied $Sr_2FeO_{4-\delta}$[2] can be made for combinations of δ and x that yield identical average Fe oxidation states (i.e., $\delta_{equiv} = x/2$). Considering one extra electron released to the system by the La^{3+}_{Sr} cation and two extra electrons released by oxygen vacancy, formally, the Fe^{3+}/Fe^{4+} concentrations can be defined as follows:

$$Sr_{2-x}La_xFe^{4+}_{1-(2\delta+x)}Fe^{3+}_{2\delta+x}O_{4-\delta} \quad (3)$$

Particularly, we can compare two cases x = 0.25 and x = 0.5 for δ = 0 with δ = 0.125 and δ = 0.25 for x = 0, respectively. Figure 5a,b compares the situation for the averaged $Fe^{3.75+}$

https://doi.org/10.1021/acs.jpcc.5c08764
J. Phys. Chem. C 2026, 130, 11001−11008

Downloaded from http://pubs.acs.org/jpccck/article-pdf/130/31/11001/6305266/acs.jpcc.5c08764.pdf by guest on 09 August 2026

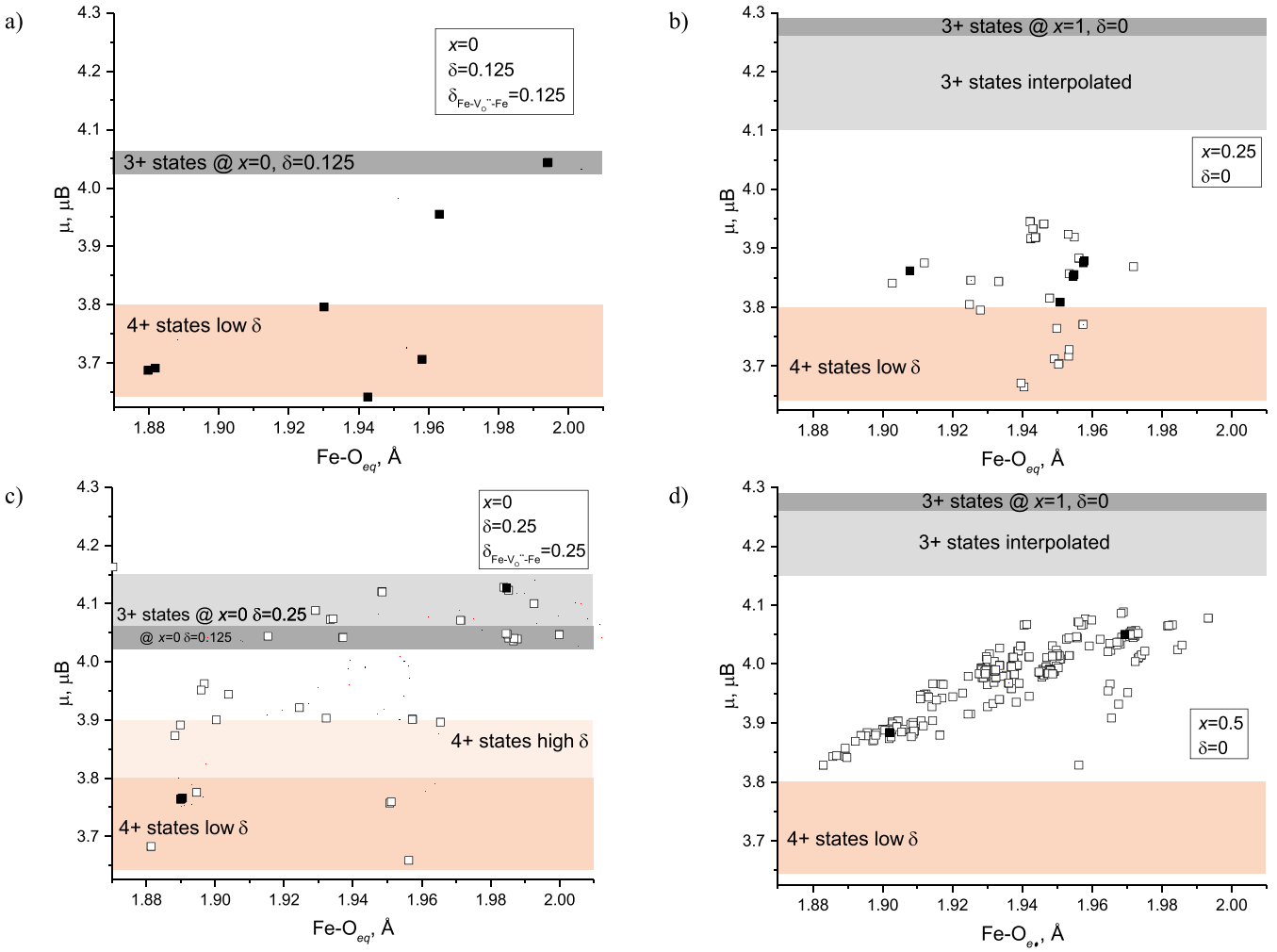


Figure 5. Magnetic moment as a function of averaged Fe−O_{eq} for average $Fe^{3.75+}$: (a) $x = 0$; $\delta = 0.125$; and (b) $x = 0.25$ $\delta = 0$. For average $Fe^{3.5+}$: (c) $x = 0$; $\delta = 0.25$; and $x = 0.5$; $\delta = 0$. For the $Sr_2FeO_{4-\delta}$ cells with $\delta > 0$, only the energetically more stable Fe−$V_O^{\bullet\bullet}$−Fe vacancy configurations are considered. Solid symbols denote the values for the lowest energy states.

state. In $Sr_2FeO_{3.875}$, one can recognize several Fe which are identified as 4+ based on magnetic moments (3.65−3.8 μ_B) and Fe−O bond length distribution[2] and others attributable as Fe^{3+}. This is in pronounced contrast to the more continuous moment distribution for $Sr_{1.75}La_{0.25}FeO_4$, where in particular no Fe reaches the Fe^{3+} zone. A similar situation is found for $Fe^{3.5+}$ in Figure 5c,d, where in $Sr_2FeO_{3.75}$ clearly a large number of Fe^{3+} and Fe^{4+} can be recognized (with larger δ, the range attributable to 4+ expands up to 3.8 μ_B,[2] shaded light red). In contrast, $Sr_{1.5}La_{0.5}FeO_4$ presents a very smooth moment distribution which does not reach the 3+ and hardly touches the 4+ zone. So, the overall conclusion is that $Sr_{2-x}La_xFeO_4$ presents a much more delocalized situation than $Sr_2FeO_{4-\delta}$. Analogously, experimental Mössbauer spectra for $Sr_{2-x}La_xFeO_4$ samples with $0.7 \leq x \leq 1.0$ were fitted with a significant fraction of a mixed 3+/4+ oxidation state.[37]

This difference can be rationalized from the following considerations. The presence of oxygen vacancies in $Sr_2FeO_{4-\delta}$ constitutes a much stronger distortion than the substitution of some Sr^{2+} by La^{3+} (although both defects lead to a decrease of the average Fe oxidation state). An oxygen vacancy causes broken Fe−O bonds, which leads to significant structural relaxations. Further, it was shown in ref 2 that the presence of an oxygen vacancy affects the electronic structure of iron in a way similar to a JT distortion (expanding two axial Fe−O bonds is not too different from completely removing one O ligand). This can stabilize localized Fe^{4+} states, and then in turn also the states accommodating the excess electrons caused by the oxygen deficiency acquire a more localized character. In contrast, such a specific driving force for forming localized Fe^{4+} states is absent in $Sr_{2-x}La_xFeO_4$. An additional reason for the more localized character of $Sr_2FeO_{4-\delta}$ might be the fact that oxygen vacancies are doubly positively charged defects (while substitutional La^{3+} has only a single relative positive charge compared to Sr^{2+}), which is expected to cause more pronounced local distortions. The strong effects of oxygen vacancies and related structural distortions have also been observed in the $SrFeO_{3-\delta}$ simple perovskites where the electronic conductivity changes from metallic character for the cubic $\delta = 0$ phase to polaron hopping in vacancy-ordered noncubic phases for $\delta > 0.03$.[38]

So, the material class of strontium ferrate perovskite and Ruddlesden−Popper phases is an intriguing example of transition-metal oxides where materials with more or less pronounced delocalized character of the electronic structure are quite close in energy. Correspondingly, small changes suffice to switch the system into one or the other direction. These may be the lattice parameter expansion in the

Downloaded from http://pubs.acs.org/jpccck/article-pdf/130/31/11001/6305266/acs.jpcc.5c08764.pdf by guest on 09 August 2026

https://doi.org/10.1021/acs.jpcc.5c08764
J. Phys. Chem. C 2026, 130, 11001−11008

$Sr_{1-x}Ba_xFeO_3$ series which induces a change from delocalized character, the absence of JT distortion, and metallic-type conductivity to a more localized character with polaron hopping for $Sr_{0.5}Ba_{0.5}FeO_3$ (or possibly already for lower Ba contents).[21]

The differences of the Fe−O bonding character are not only of fundamental interest. Preceding DFT investigations have shown that the propensity of oxides for proton uptake by water incorporation is closely coupled to the material's proton affinity and further related to the character of the O 2p states.[39] Within a $BaFeO_{3-\delta}$ supercell, O atoms opposite to an oxygen vacancy exhibit an increased covalency of the significantly shortened Fe−O bond with a decreased center of gravity of the O 2p states and correspondingly are less favorable for protonation.[25] It remains to be investigated whether a material such as $Sr_2FeO_{4-\delta}$ with distinctly different oxygen atoms (i.e., some strongly preferred protonation sites), or $Sr_{2-x}La_xFeO_4$ with more equivalent oxygens yields a higher total proton uptake (for comparable average Fe oxidation state). However, in the former, quite pronounced proton trapping effects are anticipated, which will be detrimental for a long-range proton transport.

4. CONCLUSIONS

This computational investigation of the $Sr_{2-x}La_xFeO_4$ first-order RP phase indicates that the La/Sr configurations with the shortest average La−O bond length yield the lowest total energy, and that excess energy as well as excess volume in the Sr_2FeO_4−$SrLaFeO_4$ solid solution series are negative. While La substitution decreases the average (formal) Fe oxidation state in $Sr_{2-x}La_xFeO_4$, it is not possible to identify any localized Fe^{3+} states based on magnetic moments. This is in contrast to oxygen-deficient $Sr_2FeO_{4-\delta}$ where localized Fe^{3+} species had been identified. This indicates that—for the same average Fe oxidation state—the electronic structure exhibits a more delocalized character in $Sr_{2-x}La_xFeO_4$ compared to $Sr_2FeO_{4-\delta}$. The different behavior is attributed to oxygen vacancies $V_O^{\bullet\bullet}$ (with doubly positive charge and breaking of Fe−O bonds) exerting a stronger local distortion than singly charged $La_{Sr}^{\bullet}$ and thus shifting the delicate energy balance between delocalized and more localized states toward the latter. Such differences in the electronic structure also modify the basicity of individual oxide ions and may thus affect the energetics of proton incorporation. This remains to be investigated in the future.

ASSOCIATED CONTENT

Supporting Information

The Supporting Information is available free of charge at https://pubs.acs.org/doi/10.1021/acs.jpcc.5c08764.

> Inequivalent $La_{Sr}^{\bullet}$ configurations and energetics; PAW−PBE core−electron effects; relative stability with respect to linear interpolation; $La_{Sr}^{\bullet}$−$La_{Sr}^{\bullet}$ clustering effects and A−O coordination scheme; defect interaction energies for $V_O^{\bullet\bullet}$−$La_{Sr}^{\bullet}$ complexes; Fe−O bond-length−magnetic moment correlations; Fe magnetic moments and defect-induced localization; structural and electronic parameters from HSE06 and DFT + *U*; and electronic density of states for $Sr_{2-x}La_xFeO_4$ (PDF)

AUTHOR INFORMATION

Corresponding Authors

Yuri A. Mastrikov − *Institute of Solid State Physics, University of Latvia, Riga LV-1063, Latvia; University of Maryland College Park, College Park, Maryland 20742, United States;* orcid.org/0000-0001-6867-6769; Email: yuri.mastrikov@cfi.lu.lv

Denis Gryaznov − *Institute of Solid State Physics, University of Latvia, Riga LV-1063, Latvia;* orcid.org/0000-0002-2894-4471; Email: gryaznov@cfi.lu.lv

Rotraut Merkle − *Max Planck Institute for Solid State Research, D-70569 Stuttgart, Germany;* orcid.org/0000-0003-3811-8963; Email: r.merkle@fkf.mpg.de

Authors

Andrew Chesnokov − *Institute of Solid State Physics, University of Latvia, Riga LV-1063, Latvia;* orcid.org/0000-0001-5436-8570

Guntars Zvejnieks − *Institute of Solid State Physics, University of Latvia, Riga LV-1063, Latvia;* orcid.org/0000-0001-6023-4106

Maksim Sokolov − *Institute of Solid State Physics, University of Latvia, Riga LV-1063, Latvia; University of Duisburg-Essen, D-45141 Essen, Germany*

Maija M. Kuklja − *University of Maryland College Park, College Park, Maryland 20742, United States;* orcid.org/0000-0002-5047-7734

Eugene Kotomin − *Institute of Solid State Physics, University of Latvia, Riga LV-1063, Latvia; Max Planck Institute for Solid State Research, D-70569 Stuttgart, Germany;* orcid.org/0000-0002-8122-6276

Complete contact information is available at: https://pubs.acs.org/10.1021/acs.jpcc.5c08764

Notes

The authors declare no competing financial interest.

ACKNOWLEDGMENTS

The study was performed with the financial support from the Latvian Council of Science under the grant agreement lzp-2021/1-0203. E.K., Y.M., and G.Z. thank the M-Era.Net GRIPHUS project support. The computational resources were provided by the Leibniz Supercomputing Centre (LRZ) under the grant AOECA (pn46sa) and the University of Maryland high-performance computing clusters (UMD HPCC) under the grant HPCC0001887.

REFERENCES

(1) Adler, P.; Reehuis, M.; Stüsser, N.; Medvedev, S. A.; Nicklas, M.; Peets, D. C.; Bertinshaw, J.; Christensen, C. K.; Etter, M.; Hoser, A.; Schröder, L.; Merz, P.; Schnelle, W.; Schulz, A.; Mu, Q.; Bessas, D.; Chumakov, A.; Jansen, M.; Felser, C. Spiral Magnetism, Spin Flop, and Pressure-Induced Ferromagnetism in the Negative Charge-Transfer-Gap Insulator Sr_2FeO_4. *Phys. Rev. B* **2022**, *105* (5), 54417.

(2) Mastrikov, Y. A.; Gryaznov, D.; Chesnokov, A.; Zvejnieks, G.; Sokolov, M.; Kuklja, M. M.; Merkle, R.; Kotomin, E. A. Oxygen Defect Formation and Migration in Sr2FeO4-Delta: Insights from First Principles DFT Calculations with the PBE+U Functional. *Phys. Rev. Mater.* **2025**, *9* (10), 105801.

(3) Zvejnieks, G.; Mastrikov, Y.; Gryaznov, D. Jahn−Teller Distortion in Sr2FeO4: Group-Theoretical Analysis and Hybrid DFT Calculations. *Sci. Rep.* **2023**, *13* (1), 16446.

Downloaded from http://pubs.acs.org/jpccck/article-pdf/130/31/11001/6305266/acs.jpcc.5c08764.pdf by guest on 09 August 2026

(4) Zvejnieks, G.; Mastrikov, Y.; Merkle, R.; Gryaznov, D. Competing Charge Ordering and Jahn-Teller Modes in Sr3Fe2O7: Hybrid DFT Calculations and Symmetry Mode Analysis. *Phys. Rev. B* **2025**, *112* (7), 75118.
(5) Hoedl, M. F. Electronic Structure and Defect Chemistry in Iron Perovskites; PhD Thesis; University of Stuttgart, 2021.
(6) Papac, M.; Stevanović, V.; Zakutayev, A.; O'Hayre, R. Triple Ionic−Electronic Conducting Oxides for next-Generation Electrochemical Devices. *Nat. Mater.* **2021**, *20* (3), 301−313.
(7) Merkle, R.; Hoedl, M. F.; Raimondi, G.; Zohourian, R.; Maier, J. Oxides with Mixed Protonic and Electronic Conductivity. *Annu. Rev. Mater. Res.* **2021**, *51* (1), 461−493.
(8) Cao, J.; Ji, Y.; Shao, Z. Perovskites for Protonic Ceramic Fuel Cells: A Review. *Energy Environ. Sci.* **2022**, *15* (6), 2200−2232.
(9) Xu, X.; Pan, Y.; Zhong, Y.; Ran, R.; Shao, Z. Ruddlesden−Popper Perovskites in Electrocatalysis. *Mater. Horiz.* **2020**, *7* (10), 2519−2565.
(10) Tarutin, A. P.; Lyagaeva, J. G.; Medvedev, D. A.; Bi, L.; Yaremchenko, A. A. Recent Advances in Layered Ln2NiO4+δ Nickelates: Fundamentals and Prospects of Their Applications in Protonic Ceramic Fuel and Electrolysis Cells. *J. Mater. Chem. A* **2021**, *9* (1), 154−195.
(11) Yu, N.; Bello, I. T.; Chen, X.; Liu, T.; Li, Z.; Song, Y.; Ni, M. Rational Design of Ruddlesden−Popper Perovskite Ferrites as Air Electrode for Highly Active and Durable Reversible Protonic Ceramic Cells. *Nanomicro Lett.* **2024**, *16* (1), 177.
(12) Dann, S. E.; Weller, M. T.; Currie, D. B. The Synthesis and Structure of Sr_2FeO_4. *J. Solid State Chem.* **1991**, *92* (1), 237−240.
(13) Wang, Z.; Yang, W.; Shafi, S. P.; Bi, L.; Wang, Z.; Peng, R.; Xia, C.; Liu, W.; Lu, Y. A High Performance Cathode for Proton Conducting Solid Oxide Fuel Cells. *J. Mater. Chem. A* **2015**, *3* (16), 8405−8412.
(14) Tan, W.; Huan, D.; Yang, W.; Shi, N.; Wang, W.; Peng, R.; Wu, X.; Lu, Y. A First-Principles Study on Divergent Reactions of Using a Sr3Fe2O7 Cathode in Both Oxygen Ion Conducting and Proton Conducting Solid Oxide Fuel Cells. *RSC Adv.* **2018**, *8* (47), 26448−26460.
(15) Jin, Z.; Peng, R.; Xia, Y.; Wang, Z.; Liu, W. Computational Investigation of Zn-Doped and Undoped SrEu2Fe2O7 as Potential Mixed Electron and Proton Conductors. *RSC Adv.* **2020**, *10* (66), 39988−39994.
(16) Shi, H.; Su, C.; Xu, X.; Pan, Y.; Yang, G.; Ran, R.; Shao, Z. Building Ruddlesden−Popper and Single Perovskite Nanocomposites: A New Strategy to Develop High-Performance Cathode for Protonic Ceramic Fuel Cells. *Small* **2021**, *17* (35), 2101872.
(17) Grimaud, A.; Mauvy, F.; Marc Bassat, J.; Fourcade, S.; Marrony, M.; Claude Grenier, J. Hydration and Transport Properties of the Pr2−xSrxNiO4+δ Compounds as H+-SOFC Cathodes. *J. Mater. Chem.* **2012**, *22* (31), 16017−16025.
(18) Zhong, P.; Toyoura, K.; Jiang, L.; Chen, L.; Ismail, S. A.; Hatada, N.; Norby, T.; Han, D. Protonic Conduction in La2NiO4+δ and La2-XAxNiO4+δ (A = Ca, Sr, Ba) Ruddlesden−Popper Type Oxides. *Adv. Energy Mater.* **2022**, *12* (22), 2200392.
(19) Niemczyk, A.; Merkle, R.; Maier, J.; Świerczek, K. Defect Chemistry and Proton Uptake of La2-XSrxNiO4±δ and La2-XBaxNiO4±δ Ruddlesden-Popper Phases. *J. Solid State Chem.* **2022**, *306*, 122731.
(20) Ota, T.; Morikawa, Y. Improvement of Oxygen Storage Capacity by Charge Transfer via Oxygen Ions in Sr3Fe2−XNixO7.0−δ. *Chem. Mater.* **2024**, *36* (17), 8159−8173.
(21) Hoedl, M. F.; Gryaznov, D.; Merkle, R.; Kotomin, E. A.; Maier, J. Interdependence of Oxygenation and Hydration in Mixed-Conducting (Ba,Sr)FeO3−δ Perovskites Studied by Density Functional Theory. *J. Phys. Chem. C* **2020**, *124* (22), 11780−11789.
(22) Okhotnikov, K.; Charpentier, T.; Cadars, S. Supercell Program: A Combinatorial Structure-Generation Approach for the Local-Level Modeling of Atomic Substitutions and Partial Occupancies in Crystals. *J. Cheminf* **2016**, *8* (1), 17.
(23) Kresse, G.; Furthmüller, J. Efficient Iterative Schemes for *Ab Initio* Total-Energy Calculations Using a Plane-Wave Basis Set. *Phys. Rev. B* **1996**, *54* (16), 11169−11186.
(24) Blöchl, P. E. Projector Augmented-Wave Method. *Phys. Rev. B* **1994**, *50* (24), 17953−17979.
(25) Hoedl, M. F.; Chesnokov, A.; Gryaznov, D.; Merkle, R.; Kotomin, E. A.; Maier, J. Proton Migration Barriers in $BaFeO_{3-\delta}$ − Insights from DFT Calculations. *J. Mater. Chem. A* **2023**, *11* (12), 6336−6348.
(26) Szaro, N. A.; Ammal, S. C.; Chen, F.; Heyden, A. An Ab Initio Study of the Oxygen Defect Formation and Oxide Ion Migration in $(Sr_{1-x}Pr_x)_2FeO_{4\pm\delta}$. *J. Power Sources* **2021**, *515*, 230602.
(27) Monkhorst, H. J.; Pack, J. D. Special Points for Brillouin-Zone Integrations. *Phys. Rev. B:* **1976**, *13* (12), 5188−5192.
(28) Perdew, J. P.; Burke, K.; Ernzerhof, M. Generalized Gradient Approximation Made Simple. *Phys. Rev. Lett.* **1996**, *77* (18), 3865−3868.
(29) Tang, W.; Sanville, E.; Henkelman, G. A Grid-Based Bader Analysis Algorithm without Lattice Bias. *J. Phys.: Condens. Matter* **2009**, *21* (8), 084204.
(30) Momma, K.; Izumi, F. VESTA: A Three-Dimensional Visualization System for Electronic and Structural Analysis. *J. Appl. Crystallogr.* **2008**, *41* (3), 653−658.
(31) Weizman, A.; Fuks, D.; Kotomin, E. A.; Gryaznov, D. Ab Initio Study of Phase Competition in (La1−c,Src)CoO3 Solid Solutions. *Solid State Ion* **2013**, *230*, 32−36.
(32) Fuks, D.; Bakaleinikov, L.; Kotomin, E. A.; Felsteiner, J.; Gordon, A.; Evarestov, R. A.; Gryaznov, D.; Maier, J. Thermodynamic Stability and Disordering in LacSr 1-CMnO3 Solid Solutions. *Solid State Ion* **2006**, *177* (3−4), 217−222.
(33) Fuks, D.; Dorfman, S.; Piskunov, S.; Kotomin, E. A. Ab Initio Thermodynamics of BacSr1-CTiO3 Solid Solutions. *Phys. Rev. B* **2005**, *71* (1), 14111.
(34) Merkle, R.; Hoedl, M. F.; Chesnokov, A.; Gryaznov, D.; Bucher, E.; Kotomin, E. A.; Sitte, W.; Maier, J. Electronic Structure, Phase Formation, and Defect Distribution in the Ba(Ce,Fe,Acc)O3-δ System. *Acta Mater.* **2025**, *287*, 120739.
(35) Takeda, Y.; Imayoshi, K.; Imanishi, N.; Yamamoto, O.; Takano, M. Preparation and Characterization of Sr2 − LaFeO4(0 ⩽x⩽ 1). *J. Mater. Chem.* **1994**, *4* (1), 19−22.
(36) Krukau, A. V.; Vydrov, O. A.; Izmaylov, A. F.; Scuseria, G. E. Influence of the Exchange Screening Parameter on the Performance of Screened Hybrid Functionals. *J. Chem. Phys.* **2006**, *125* (22), 224106.
(37) Jennings, A. J.; Skinner, S. J.; Helgason, O. ·. Structural Properties of LaxSr2−xFeO4±δ at High Temperature and under Reducing Conditions. *J. Solid State Chem.* **2003**, *175* (2), 207−217.
(38) Mizusaki, J.; Okayasu, M.; Yamauchi, S.; Fueki, K. Nonstoichiometry and Phase Relationship of the SrFeO2.5SrFeO3 System at High Temperature. *J. Solid State Chem.* **1992**, *99* (1), 166−172.
(39) Bjørheim, T. S.; Hoedl, M. F.; Merkle, R.; Kotomin, E. A.; Maier, J. Proton, Hydroxide Ion, and Oxide Ion Affinities of Closed-Shell Oxides: Importance for the Hydration Reaction and Correlation to Electronic Structure. *J. Phys. Chem. C* **2020**, *124* (2), 1277−1284.

Downloaded from http://pubs.acs.org/jpccck/article-pdf/130/31/11001/6305266/acs.jpcc.5c08764.pdf by guest on 09 August 2026

https://doi.org/10.1021/acs.jpcc.5c08764
J. Phys. Chem. C 2026, 130, 11001−11008